Nanoscale Advances

ROYAL SOCIETY OF CHEMISTRY

PAPER

View Article Online
View Journal | View Issue

Cite this: *Nanoscale Adv.*, 2020, **2**, 1949

On the formation of superoxide radicals on colloidal $ATiO_3$ (A = Sr and Ba) nanocrystal surfaces†

Muhammad Abdullah, Ruby J. Nelson and Kevin R. Kittilstved *

Received 7th February 2020
Accepted 15th April 2020

DOI: 10.1039/d0na00106f

rsc.li/nanoscale-advances

Controlling the surface chemistry of colloidal semiconductor nanocrystals is critical to exploiting their rich electronic structures for various technologies. We recently demonstrated that the hydrothermal synthesis of colloidal nanocrystals of $SrTiO_3$, a technologically-relevant electronic material, provided a strong negative correlation between the presence of an O_2-related surface defect and hydrazine hydrate [W. L. Harrigan, S. E. Michaud, K. A. Lehuta, and K. R. Kittilstved, *Chem. Mater.*, 2016, **28**(2), 430]. When hydrazine hydrate is omitted during the aerobic hydrothermal synthesis, the surface defect is observed. However, it can be removed by either the addition of hydrazine hydrate or by purging the reaction solution with argon gas before the hydrothermal synthesis. We also propose that the formation of the O_2-related defect is mediated by the reduction of dissolved O_2 by lactate anions that are present from the titanium precursor. This work helps elucidate the nature of the O_2-related defect as a superoxide anion ($O_2^{\bullet-}$) and presents a mechanism to explain its formation during the hydrothermal synthesis of $SrTiO_3$ and related $BaTiO_3$ nanocrystals.

Introduction

$SrTiO_3$ and $BaTiO_3$ are wide-gap semiconductors that have received much attention due to their rich defect chemistries that enable a wide range of electrical properties from insulating to metallic.[1] In addition to exhibiting prototypical quantum paraelectric behavior,[2] these semiconductors are also promising host lattices for visible-light photocatalytic H_2O splitting and CO_2 reduction,[3–9] sensors,[10] and memristors.[11,12] Recent advances in the colloidal synthesis[13–20] of ternary metal oxide nanocrystals (NCs) including $SrTiO_3$ and $BaTiO_3$ has generated further interest in the emergent phenomena that arise in these technologically-relevant materials when prepared with nanometer dimensions.

Most of the interesting applications of bulk $SrTiO_3$ results from the presence of two native n-type defects: oxygen vacancies (V_O) and self-trapped Ti^{3+} ions. These defects increase the carrier density and mid-gap trapped states which give rise to tunable blue light emission[21] but also greatly influence light absorption in the visible region that has been shown to enhance photocatalytic performance in bulk powders.[22] For example, superoxide radicals ($O_2^{\bullet-}$) present on the surface of Ti(IV)-based metal oxides play an essential role in photocatalysis and degradation of organic pollutants.[23–25] These $O_2^{\bullet-}$ are generally produced by post-synthetic treatments of reduced titanium oxide-based materials with molecular oxygen (O_2) or H_2O_2. Yu *et al.* generated surface $O_2^{\bullet-}$ by injecting electrons from photoinduced excited states into adsorbed O_2 on the surface of colloidal TiO_2 nanoparticles.[26] Another potential use of $O_2^{\bullet-}$ is the catalytical decomposition of H_2O_2 on the surface of titanium oxides[27] and oxidative coupling of alkyl radicals.[28] In most of these cases, the metal oxide surface needs to be activated prior to $O_2^{\bullet-}$ formation by irradiation or suitable chemical treatments.

We recently reported the synthesis[29] of colloidal $SrTiO_3$ NCs by modified hydrothermal methods[15,17,18] that are readily suspended in non-polar solvents. Electron paramagnetic resonance (EPR) and optical spectroscopies showed that the $SrTiO_3$ NCs can display spectroscopic signatures that were assigned to an oxygen-related surface defect that is sensitive to the presence of hydrazine hydrate during synthesis. However, the role of hydrazine in the formation of this surface defect remained speculative. Hydrazine has been previously used as an additive during the hydrothermal synthesis of $SrTiO_3$ and $BaTiO_3$ NCs. Sun and co-workers have studied the absorption of hydrazine on the surface of $BaTiO_3$ nanoparticles.[30] Experimental and simulation analysis indicated that only amorphous $BaTiO_3$ particles are obtained without the addition of hydrazine. Similarly, Fujinami *et al.* claimed that $SrTiO_3$ NCs without cubic shape were obtained when synthesis was carried out in the absence of hydrazine.[17] However, our recent report presented evidence that near-cubic colloidal $SrTiO_3$ NCs can be prepared with or without the addition of hydrazine.[29]

Department of Chemistry, University of Massachusetts Amherst, 710 N Pleasant St, Amherst, MA, 01003, USA. E-mail: kittilstved@chem.umass.edu

† Electronic supplementary information (ESI) available. See DOI: 10.1039/d0na00106f

Herein we report a systemic investigation of this correlation between hydrazine and the presence of this surface defect in colloidal $SrTiO_3$ NCs. We hypothesize that the hydrazine may scavenge molecular O_2 inside the closed reaction vessel during synthesis, thus providing an inert atmosphere that would inhibit $O_2^{\bullet-}$ formation on the NC surface. To test the role of hydrazine, we performed the hydrothermal synthesis both with and without hydrazine prepared in ambient conditions, and also without hydrazine but under anaerobic conditions after purging the reaction solution with argon gas. Reactions performed with hydrazine or under anaerobic conditions produced the same observations and strongly suggest that hydrazine is indeed removing O_2 inside the closed reaction vessel. These experiments also strengthen our assignment of the surface-related defect species as $O_2^{\bullet-}$ ions for the $SrTiO_3$ NCs samples prepared aerobically without hydrazine. We propose that lactate ligands of the Ti(IV) precursor reduce O_2 to $O_2^{\bullet-}$ ions during the hydrothermal synthesis (200 °C and basic conditions). To support this mechanism and generality of $O_2^{\bullet-}$ formation and the importance of lactate ions, we prepared $BaTiO_3$ NCs from the same lactate-containing Ti(IV) precursors as well as a lactate-free precursor. $O_2^{\bullet-}$ defects are observed only in NCs prepared from precursor that contain lactate ligands under aerobic conditions. These results provide convincing evidence that the choice of precursor can lead to unique surface chemistry and the formation of $O_2^{\bullet-}$ defects on titanate-based NCs.

Experimental

Materials

Strontium hydroxide octahydrate ($Sr(OH)_2 \cdot 8H_2O$, 99%, Alfa Aesar), barium hydroxide octahydrate ($Ba(OH)_2 \cdot 8H_2O$, 99.95%, Acros Organics), titanium(IV) bis(ammonium lactate) dihydroxide (TALH, 50% in water, Alfa Aesar), titanium(IV) *tert*-butoxide ($Ti(OBu)_4$, 99%, Acros Organics), 1-butanol (99%, Acros Organics), tetramethylammonium hydroxide (NMe_4OH, Acros Organics), sodium hydroxide (NaOH, Certified ACS, Fisher Chemical), hydrazine hydrate (99%, Acros Organics), oleic acid (90%, Fisher Chemical), oleylamine (50%, TCI America), ethanol (200 proof, PHARMCO-AAPER) and hexanes (optima grade, Fisher Chemicals) were all used as received.

Synthesis of colloidal $SrTiO_3$ NCs from TALH

Synthesis of colloidal $SrTiO_3$ NCs was carried out by the hydrothermal method as reported previously by our group.[29] In a typical procedure, 1.25 mmol of each of TALH and $Sr(OH)_2$ were dissolved in 30 mL of distilled water in 45 mL Teflon-lined autoclave. The pH of the solution was then adjusted to 12.1 with a 10 M NMe_4OH solution followed by the addition of oleic acid (2.5 mmol). The reaction vessel was then sealed and heated to 200 °C in oven for 24 hours. The resulting NCs were collected, washed with ethanol three times and suspended in hexanes. This procedure described above is referred herein as method-I.

Method-I was modified to prepare two different sets of colloidal NCs. In the first modification referred to as method-II, hydrazine hydrate (5 mmol) was added in reaction mixture before adding oleic acid. The pH of the solution remained at 12.1 after addition of hydrazine hydrate. The last modification, method-III, was identical to method-I but the reaction solution was purged with argon gas for 60 minutes prior to closing the Teflon-lined reaction vessel.

Synthesis of colloidal $BaTiO_3$ NCs from TALH

Synthesis of colloidal $BaTiO_3$ NCs was also carried out by a similar hydrothermal method and TALH precursor but included constant magnetic stirring. In a typical preparation, 1.5 mmol of each TALH and $Ba(OH)_2$ were dissolved in 24 mL distilled water followed by addition of 6 mL of NaOH (5 M). The reaction solution was then transferred to a 45 mL Teflon-lined autoclave and oleylamine (6 mmol) and oleic acid (6 mmol) were added. The pH of the reaction solution was 12. The sealed autoclave was placed in custom-made aluminum block housing that was heated to 215 °C and stirred constantly for 24 h using a stirring hotplate. After the synthesis, autoclave was cooled to room temperature and the solid product was collected, washed with EtOH, and dissolved in nonpolar solvents such hexanes to produce a transparent solution. This procedure described above is referred herein as method-A. The method-A was modified to prepare another set of $BaTiO_3$ NCs referred as method-B. In this modification, hydrazine hydrate (5 mmol) was added before adding the oleylamine and oleic acid. Method-A and -B for $BaTiO_3$ mimics method-I and -II for the $SrTiO_3$ NCs.

Synthesis of $BaTiO_3$ NCs from $Ti(OBu)_4$

Synthesis of lactate-free $BaTiO_3$ NCs was done using an aerobic hydrothermal method adopted from literature.[31] In a typical experiment, aqueous solutions containing 1 mmol of $Ba(OH)_2$ dissolved in 5 mL water and 12.5 mmol of NaOH dissolved in 5 mL water were mixed with 10 mL of 1-butanol containing 1 mmol $Ti(OBu)_4$ and 2.5 mL of oleic acid. The pH of the solution was 12.2. The resulting precursor solution was transferred to a 45 mL autoclave, closed under ambient conditions, and heated to 180 °C for 18 hours. The resulting product was collected, washed with EtOH several times and dispersed in non-polar solvents such as hexanes.

Physical characterization

All measurements were collected at room-temperature unless specified otherwise. Electronic absorption spectra were collected on colloidal suspensions in air-tight quartz cuvettes with 1 cm pathlengths (Cary 50 Bio). EPR spectra were measured at X-band frequency (9.6 GHz) with a Bruker Elexsys-500 equipped with a Super High QE (ER4123SHQE) cavity. Transmission electron microscopy (TEM) images of NCs deposited onto copper grids (CF400-CU-50, Electron Microscopy Sciences) with a 3 nm carbon coating (JEOL TEM-2000FX). Powder X-ray diffraction patterns were collected in the Bragg–Brentano configuration with a Cu Kα source (Rigaku SmartLab SE). FTIR spectra were collected using Bruker Alpha-P equipped with a diamond attenuated total reflectance (ATR) crystal. High resolution electrospray ionization mass spectra (ESI-MS) were collected in negative ion mode with Bruker MicroTOF-II. In

a typical sample preparation for ESI-MS, the aqueous reaction mixture from the hydrothermal synthesis was centrifuged to separate NCs from the rest of the water-soluble side-products. The aqueous supernatant was used for ESI-MS measurements with no further purification.

Results and discussion

The crystallinity and phase purity of the $SrTiO_3$ NCs was confirmed by powder X-ray diffraction (see ESI†). All samples matched to cubic $SrTiO_3$ in the $Pm\bar{3}m$ space group.[32] The similar powder patterns among the samples suggests that modification of hydrothermal synthesis either by adding hydrazine hydrate or degassing the precursor solution has no effect on the crystalline phase or phase purity. TEM images also demonstrate cuboidal morphology of the $SrTiO_3$ NCs prepared by method-III in agreement with previously reported NC shapes made by method-I or method-II (see ESI†).[29]

FTIR absorption measurements collected on $SrTiO_3$ NCs prepared from each method are shown in Fig. 1. The prominent peaks at 1540 cm^{-1} and 1450 cm^{-1} correspond to the symmetric and asymmetric stretches of the bound carboxylate head group of the surface oleate ligand and is observed in each sample. Aliphatic bands from the oleate surface ligands also appear *ca.* 2900 cm^{-1}. All samples thus indicate the NC surfaces are passivated by oleate ligands within the sensitivity of the instrument. These spectra are similar to prior reports of $SrTiO_3$ made in the similar method[17] but at pH 13.5. There is no evidence of N–H stretches from hydrazine in the NCs prepared by method-II that would appear around 3400 cm^{-1}.[33] This observation suggests that hydrazine is not being adsorbed on the surface of $SrTiO_3$ NCs. Furthermore, hydrazine adsorption is not expected as it is known to decompose rapidly at this reaction temperature (200 °C) in the presence of oxygen to possible products of N_2 and H_2O.[34] Fujinami *et al.* also observed essentially no change in pH of the reaction solution after $SrTiO_3$ NC synthesis regardless of whether hydrazine was present, which was speculated to play a different role than decomposing to NH_3.[17]

The electronic absorption spectrum of all colloidal $SrTiO_3$ NCs dispersed in hexanes is dominated by the band edge absorption at *ca.* 3.25 eV consistent with bulk $SrTiO_3$ (see Fig. 2).[35] However, NCs prepared by the aerobic hydrothermal method-I also exhibit broad absorption throughout the entire visible region and appear reddish-brown (see color photographs shown in Fig. 2 inset). The broad sub-bandgap absorption is absent in $SrTiO_3$ samples prepared using either method-II or method-III.

The origin of the visible absorption in method-I NCs suggests the presence of defects with sub-bandgap levels. Native point defects such as V_O or Ti^{3+} are also known to give rise to visible light absorption in bulk $SrTiO_3$. Electronic transitions from the valence band to different V_O charge states have been observed between 450 and 550 nm.[36–38] Rice *et al.* recently attributed a transition involving the V_O to an absorption band at *ca.* 405 nm in reduced $SrTiO_3$ crystals.[39] Similar V_O defects have also been described as polarons. However, the electronic transition of the localized electron trapped on Ti^{3+} sites to the conduction band minimum is broad and centered in the near-IR region.[40,41] To explore the origin of the brownish coloration of the $SrTiO_3$ NCs prepared by method-I, we carried out EPR spectroscopy measurements on all three types of $SrTiO_3$ NCs.

The room temperature, X-band EPR spectrum of the $SrTiO_3$ NCs prepared by method-I is shown in Fig. 3. These NCs exhibit a narrow resonance near 351 mT corresponding to *g*-value of 2.003. Upon addition of hydrazine (method-II) or purging the precursors with argon (method-III), this EPR signal disappears. Carter *et al.* have identified four types of oxygen-related defects on the surface of TiO_2 (anatase-type) using EPR spectroscopy and the signal at $g = 2.003$ was assigned to surface-adsorbed paramagnetic superoxide radicals ($O_2^{\bullet-}$, $S = 1/2$).[42] Those

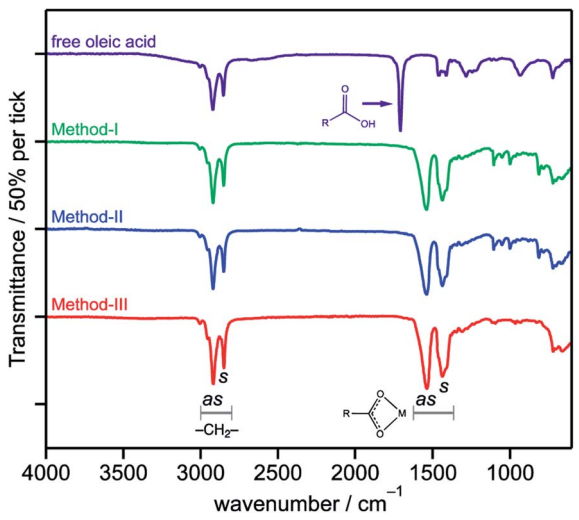

Fig. 1 FTIR spectra of solvent-evaporated $SrTiO_3$ NCs prepared by method-I (green), method-II (blue) and method-III (red). The top spectrum belongs to oleic acid (purple). The s and as next to the peaks refer to the symmetric and asymmetric stretches associated with the aliphatic C–H or carboxylate vibrations.

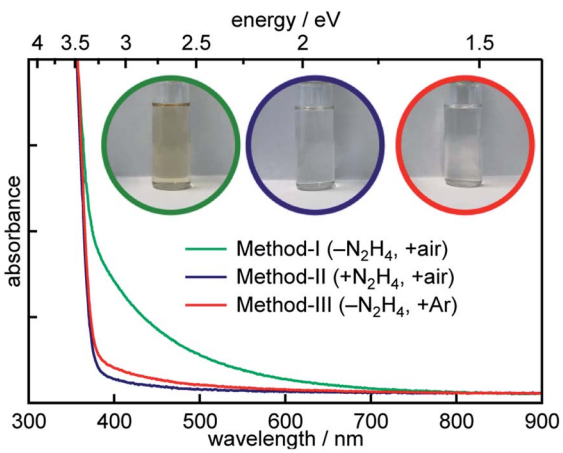

Fig. 2 Electronic absorption spectra of colloidal $SrTiO_3$ NCs dispersed in hexanes prepared by method-I (green), method-II (blue) and method-III (red). Optical densities were matched at ~350 nm. Color photographs of NCs dispersed in hexanes are shown in insets.

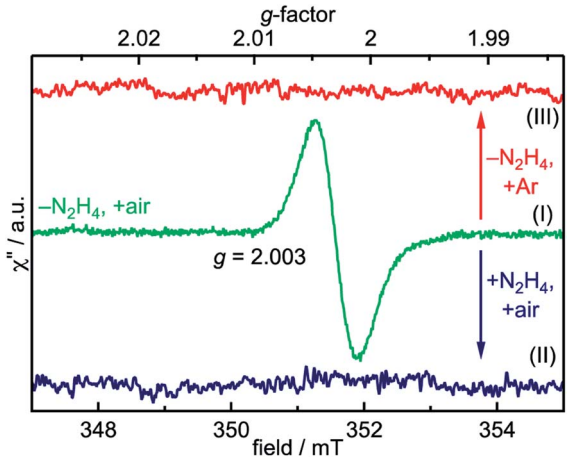

Fig. 3 Room temperature EPR spectra of NCs prepared by method-I (middle/green), method-II (bottom/blue), and method-III (top/red).

authors also propose the formation involves electron transfer from trapped electrons at Ti^{3+} sites to surface-O_2 to produce $O_2^{\bullet-}$. We also tentatively assigned the $g = 2.003$ signal to $O_2^{\bullet-}$ in our initial report on the synthesis and characterization of $SrTiO_3$ NCs.[29] We also demonstrated in a more recent report that this $g = 2.003$ signal can be increased upon exposing photochemically reduced (Ti^{3+}-rich) Cr^{3+}-doped $SrTiO_3$ NCs to air.[41] Others have also reported a TiO_2-based NCs treated with H_2O_2 that display similar absorption in the visible region originating from surface-adsorbed $O_2^{\bullet-}$ defects.[43,44] Based on the similarity to previous reports and observations,[41,43] we attribute the reddish-brown coloration and EPR resonance at $g = 2.003$ observed in Fig. 2 and 3, respectively, to the presence of $O_2^{\bullet-}$ radicals on the surface of $SrTiO_3$ NCs prepared under aerobic hydrothermal conditions (method-I). We further assign the visible absorption to defect-induced sub-bandgap states that give rise to charge transfer-like transitions.

Our working hypothesis is that the $O_2^{\bullet-}$ ions are formed *via* reduction of dissolved O_2 during the hydrothermal synthesis. The lack of $O_2^{\bullet-}$ formation when prepared by either method-II or method-III is thus presumably due to a very low O_2 content in the reaction solution during the hydrothermal synthesis. Despite these results, we do not have a direct mechanistic understanding of how the $O_2^{\bullet-}$ is formed during synthesis. One outstanding question that we sought to answer is the identity of the electron donor. The $O_2^{\bullet-}$ formation at TiO_2 surfaces is believed to proceed *via* electron transfer from Ti^{3+} sites to adsorbed O_2.[45,46] In bulk $SrTiO_3$, oxygen vacancies are thought to exist between adjacent localized Ti^{3+} sites,[47,48] which could serve as an electron donor. However, no spectroscopic evidence for the existence of V_O and any localized Ti^{3+} defects were found in $SrTiO_3$ colloidal NCs. It is possible that these species are only formed under hydrothermal conditions during synthesis but suggests the presence of an alternative electron donors such as lactate ions.

The hydrothermal synthesis of $SrTiO_3$ NCs involves the hydrolysis of titanium(IV) bis(ammonium lactato) dihydroxide (TALH) as the titanium source under basic conditions. Möckel *et al.* have proposed that the hydrolysis of TALH to form TiO_2 NCs produces free ammonium lactate in neutral or slightly acidic conditions.[49] Seisenbaeva *et al.* have proposed hydrolysis of TALH forms a stable, tetrameric $(NH_4)_8Ti_4O_4(lactate)_8$ cluster that serves as a precursor to the formation of TiO_2 NCs under basic conditions.[50] In both of above mentioned references, lactate ions are commonly observed as hydrolysis by-product. Lactate ions have been shown to serve as electron donors in various chemical and biological systems to produce O_2-based radicals.[51,52] Therefore, we hypothesize that the lactate ions reduce dissolved O_2 under extremely high pH to produce $O_2^{\bullet-}$ and the corresponding by-product pyruvate anions as described by Scheme 1.

In Scheme 1, we depict $ATiO_3$ surface that is stabilized by oleate ligands under hydrothermal conditions (pH 12 and 200 °C). At this high temperature, we expect the surface ligands to rapidly exchange between bound and free. This dynamics surface would allow for $O_2^{\bullet-}$ to bind to the surface in method-I and become stabilized upon cooling to room temperature. In the anaerobic cases, method-II and method-III, there is no direct way to produce $O_2^{\bullet-}$ in solution and therefore rule out the possibility of $O_2^{\bullet-}$ adsorption on NC surface.

To confirm the presence of lactate and pyruvate anions, we performed mass spectrometry analysis of reaction supernatants from the various syntheses without purification. Fig. 4 shows a zoomed in region of the negative ion mode ESI-MS spectra collected from all three methods. The dominant peak at m/z 89 is attributed to lactate ions which are formed in all three methods consistent with our hypothesis. Despite being weak, the presence of a minority peak at m/z 87 is detected in each of the samples and corresponds to pyruvate ions. When normalized to the lactate signals for the three methods, we detect about a three-fold higher relative intensity of pyruvate anion signal from the supernatant from method-I. While not absolutely quantitative, the ESI-MS results suggest this conversion yield is <1%. Despite this limitation, the observation is consistent with the proposed mechanism that at least some fraction of the lactate ions undergoes the conversion shown in Scheme 1. The

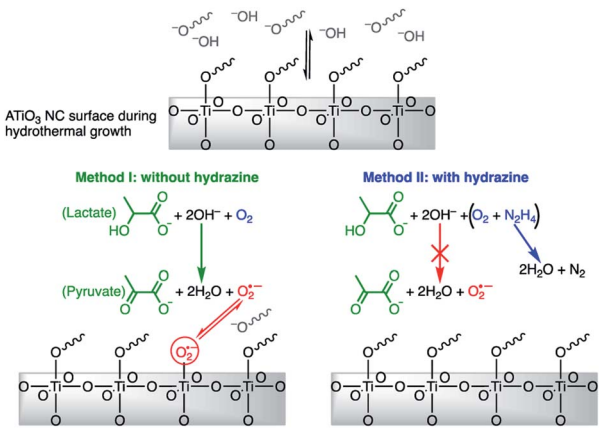

Scheme 1 Proposed mechanism of superoxide formation and adsorption onto the dynamic $ATiO_3$ surface during the hydrothermal synthesis.

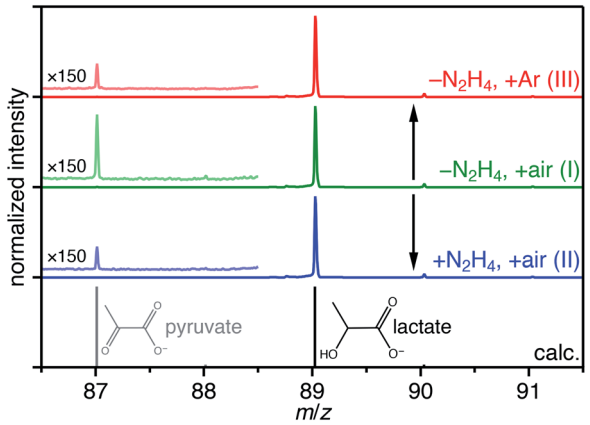

Fig. 4 Negative-ion mode ESI-MS of supernatants from the various reactions in the region of the lactate ($[C_3H_5O_3]^{\bullet-}$) and pyruvate ($[C_3H_3O_3]^{\bullet-}$) anions. The spectra are normalized to the major peak from the lactate anion at *m/z* 89.

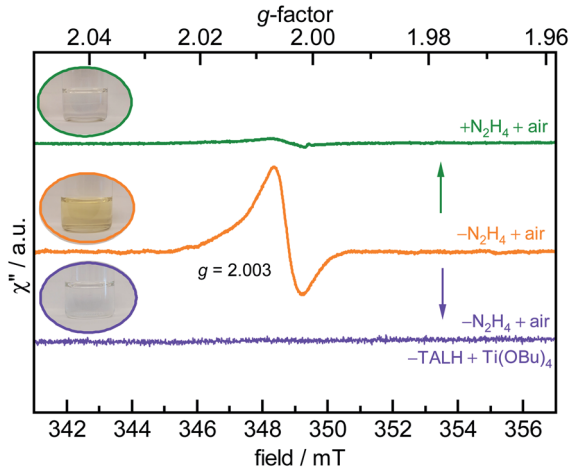

Fig. 5 Room temperature EPR spectra of $BaTiO_3$ NCs prepared without hydrazine (orange/middle), with hydrazine (top/green) and from lactate-free precursor (bottom/purple). All samples were prepared in air. The color photographs of colloidal solution in hexanes for NCs prepared from all three methods are shown in insets.

lower O_2 content in method-III precludes the $O_2^{\bullet-}$ formation which in turn can be supported by observing relatively a lower pyruvate concentration. However, the absence of any $O_2^{\bullet-}$ defects together with much lower pyruvate content in method-II questions the role of hydrazine in controlling the $O_2^{\bullet-}$ formation during hydrothermal synthesis.

Based on results above, hydrazine appears to control the formation of $O_2^{\bullet-}$ defects by limiting the available O_2 in the synthesis. Hydrazine has been used to remove O_2 in industrial-scale reactors for decades.[53,54] The reaction between hydrazine and O_2 produces N_2 and $2H_2O$, which provides the inert atmosphere during synthesis as shown in Scheme 1.[34] Post-synthetic attempts to control the concentration of defects on the surface of the $SrTiO_3$ NCs prepared by method-I were also performed. When an excess of hydrazine hydrate is added to an aqueous mixture of defect-rich NCs and heated under aerobic hydrothermal conditions, no change in the appearance of the NCs was observed suggesting no change in surface defects (data not shown).

To test the generality of this approach, we extended the study to $BaTiO_3$ NCs using a similar hydrothermal-based synthesis with TALH and a literature solvothermal method (see ESI†). The room temperature EPR spectra of $BaTiO_3$ NCs prepared from all methods is shown in Fig. 5. Similar to the results for $SrTiO_3$, the appearance of a $O_2^{\bullet-}$ resonance at $g = 2.003$ is observed in $BaTiO_3$ samples prepared using TALH and air. The formation of these $O_2^{\bullet-}$ defects can be inhibited by adding hydrazine to remove O_2 from the reaction that is consistent with our proposed mechanism.

To confirm the critical role of lactate ions in the formation of these surface $O_2^{\bullet-}$ defects, we synthesized $BaTiO_3$ NCs from a lactate-free titanium precursor, $Ti(OBu)_4$, using similar hydrothermal conditions as used above with TALH.[31] The resulting lactate-free $BaTiO_3$ NCs are transparent below the band gap and do not display any detectable EPR signal as shown in Fig. 5 and in the ESI.† This result is entirely consistent with the critical role that lactate ions play in the formation of $O_2^{\bullet-}$ defects during hydrothermal synthesis of $ATiO_3$ and likely also TiO_2 NCs.

Conclusions

In conclusion, we have presented a systemic study of the surface defects formed during the hydrothermal synthesis of colloidal $SrTiO_3$ and $BaTiO_3$ NCs. We found that an electron transfer step presumably from lactate anions (from the Ti^{4+} precursor) to dissolved O_2 may be the key step that leads to the formation of the surface-adsorbed $O_2^{\bullet-}$ ions under these reaction conditions (high pH and high temperature). These surface $O_2^{\bullet-}$ defects are EPR active and impart a broad feature throughout the visible region that produces a reddish-brown color to the NCs. We also provided evidence that the removal of dissolved O_2 by either (1) addition of hydrazine, (2) purging with argon, or (3) using lactate-free Ti(IV) precursors inhibit $O_2^{\bullet-}$ formation. These results shed light on the role of additives in the chemical synthesis of colloidal $ATiO_3$ NCs and we are currently investigating the generality of this approach to control the formation of O_2-related surface defects in other colloidal metal oxide NCs. Modification of these surface defects through post-synthetic treatments are currently underway.

Conflicts of interest

The authors declare that this research was conducted in the absence of any commercial or financial relationships that could be constructed as a potential conflict of interest.

Acknowledgements

This work was supported by the U.S. National Science Foundation (DMR-1747593). The acquisition of the powder X-ray diffractometer used in this work was supported by the U.S.

National Science Foundation Major Research Instrumentation program (CHE-1726578). R. J. N. acknowledges support through the NSF REU Program (CHE-1659266). We acknowledge Prof. Dhandapani Venkataraman at the University of Massachusetts Amherst for use of the FTIR spectrophotometer. We also thank Blaise Arden and Jillian Denhardt for ESI-MS measurements, and Dr William Harrigan for fruitful discussions in the early stages of this project.

Notes and references

1 J. Son, P. Moetakef, B. Jalan, O. Bierwagen, N. J. Wright, R. Engel-Herbert and S. Stemmer, Epitaxial $SrTiO_3$ films with electron mobilities exceeding 30 000 $cm^2 V^{-1} s^{-1}$, *Nat. Mater.*, 2010, **9**, 482.

2 K. Müller and H. Burkard, $SrTiO_3$: An intrinsic quantum paraelectric below 4 K, *Phys. Rev. B*, 1979, **19**(7), 3593.

3 Q. Wang, T. Hisatomi, Q. Jia, H. Tokudome, M. Zhong, C. Wang, Z. Pan, T. Takata, M. Nakabayashi, N. Shibata, Y. Li, I. D. Sharp, A. Kudo, T. Yamada and K. Domen, Scalable water splitting on particulate photocatalyst sheets with a solar-to-hydrogen energy conversion efficiency exceeding 1%, *Nat. Mater.*, 2016, **15**(6), 611.

4 S. Shoji, A. Yamaguchi, E. Sakai and M. Miyauchi, Strontium titanate based artificial leaf loaded with reduction and oxidation cocatalysts for selective CO_2 reduction using water as an electron donor, *ACS Appl. Mater. Interfaces*, 2017, **9**(24), 20613.

5 T. K. Townsend, N. D. Browning and F. E. Osterloh, Nanoscale strontium titanate photocatalysts for overall water splitting, *ACS Nano*, 2012, **6**(8), 7420.

6 H. Kato and A. Kudo, Visible-light-response and photocatalytic activities of TiO_2 and $SrTiO_3$ photocatalysts codoped with antimony and chromium, *J. Phys. Chem. B*, 2002, **106**(19), 5029.

7 T. Ishii, H. Kato and A. Kudo, H_2 evolution from an aqueous methanol solution on $SrTiO_3$ photocatalysts codoped with chromium and tantalum ions under visible light irradiation, *J. Photochem. Photobiol., A*, 2004, **163**(1–2), 181.

8 R. Niishiro, H. Kato and A. Kudo, Nickel and either tantalum or niobium-codoped TiO_2 and $SrTiO_3$ photocatalysts with visible-light response for H_2 or O_2 evolution from aqueous solutions, *Phys. Chem. Chem. Phys.*, 2005, **7**(10), 2241.

9 H. Kato, Y. Sasaki, N. Shirakura and A. Kudo, Synthesis of highly active rhodium-doped $SrTiO_3$ powders in Z-scheme systems for visible-light-driven photocatalytic overall water splitting, *J. Mater. Chem. A*, 2013, **1**(39), 12327.

10 N. Sarin, M. Mishra, G. Gupta, I. P. Parkin and V. Luthra, Elucidating iron doping induced n- to p- characteristics of strontium titanate based ethanol sensors, *Curr. Appl. Phys.*, 2018, **18**(2), 246.

11 C. Baeumer, C. Schmitz, A. H. Ramadan, H. Du, K. Skaja, V. Feyer, P. Muller, B. Arndt, C. L. Jia, J. Mayer, R. A. De Souza, C. Michael Schneider, R. Waser and R. Dittmann, Spectromicroscopic insights for rational design of redox-based memristive devices, *Nat. Commun.*, 2015, **6**, 8610.

12 J. Wang, S. Choudhary, W. L. Harrigan, A. J. Crosby, K. R. Kittilstved and S. S. Nonnenmann, Transferable memristive nanoribbons comprising solution-processed strontium titanate nanocubes, *ACS Appl. Mater. Interfaces*, 2017, **9**(12), 10847.

13 C. W. Beier, M. A. Cuevas and R. L. Brutchey, Low-temperature synthesis of solid-solution $Ba_xSr_{1-x}TiO_3$ nanocrystals, *J. Mater. Chem.*, 2010, **20**(24), 5074.

14 Q. Ma and K. Kato, Nucleation and growth mechanism of barium titanate nanoblocks in hydrothermal process using aqueous titanium compound, *Cryst. Growth Des.*, 2017, **17**(5), 2507.

15 F. Dang, K.-I. Mimura, K. Kato, H. Imai, S. Wada, H. Haneda and M. Kuwabara, Growth of monodispersed $SrTiO_3$ nanocubes by thermohydrolysis method, *CrystEngComm*, 2011, **13**(11), 3878.

16 G. Canu and V. Buscaglia, Hydrothermal synthesis of strontium titanate: thermodynamic considerations, morphology control and crystallisation mechanisms, *CrystEngComm*, 2017, **19**(28), 3867.

17 K. Fujinami, K. Katagiri, J. Kamiya, T. Hamanaka and K. Koumoto, Sub-10 nm strontium titanate nanocubes highly dispersed in non-polar organic solvents, *Nanoscale*, 2010, **2**(10), 2080.

18 K. Park, J. S. Son, S. I. Woo, K. Shin, M.-W. Oh, S.-D. Park and T. Hyeon, Colloidal synthesis and thermoelectric properties of La-doped $SrTiO_3$ nanoparticles, *J. Mater. Chem. A*, 2014, **2**(12), 4217.

19 S. O'Brien, L. Brus and C. B. Murray, Synthesis of monodisperse nanoparticles of barium titanate: toward a generalized strategy of oxide nanoparticle synthesis, *J. Am. Chem. Soc.*, 2001, **123**(48), 12085.

20 F. A. Rabuffetti and R. L. Brutchey, Complex perovskite oxide nanocrystals: low-temperature synthesis and crystal structure, *Dalton Trans.*, 2014, **43**(39), 14499.

21 D. Kan, T. Terashima, R. Kanda, A. Masuno, K. Tanaka, S. Chu, H. Kan, A. Ishizumi, Y. Kanemitsu, Y. Shimakawa and M. Takano, Blue-light emission at room temperature from Ar^+-irradiated $SrTiO_3$, *Nat. Mater.*, 2005, **4**(11), 816.

22 H. Tan, Z. Zhao, W. B. Zhu, E. N. Coker, B. Li, M. Zheng, W. Yu, H. Fan and Z. Sun, Oxygen vacancy enhanced photocatalytic activity of pervoskite $SrTiO_3$, *ACS Appl. Mater. Interfaces*, 2014, **6**(21), 19184.

23 D. Wang, L. Zhao, H. Ma, H. Zhang and L. H. Guo, Quantitative analysis of reactive oxygen species photogenerated on metal oxide nanoparticles and their bacteria toxicity: The role of superoxide radicals, *Environ. Sci. Technol.*, 2017, **51**(17), 10137.

24 Y. Li, W. Zhang, J. Niu and Y. Chen, Mechanism of photogenerated reactive oxygen species and correlation with the antibacterial properties of engineered metal-oxide nanoparticles, *ACS Nano*, 2012, **6**(6), 5164.

25 M. Hayyan, M. A. Hashim and I. M. AlNashef, Superoxide ion: Generation and chemical implications, *Chem. Rev.*, 2016, **116**(5), 3029.

26 J. Yu, J. Chen, C. Li, X. Wang, B. Zhang and H. Ding, ESR signal of superoxide radical anion adsorbed on TiO_2

generated at room temperature, *J. Phys. Chem. B*, 2004, **108**(9), 2781.

27 S. Mumtaz, L. S. Wang, S. Z. Hussain, M. Abdullah, Z. Huma, Z. Iqbal, B. Creran, V. M. Rotello and I. Hussain, Dopamine coated Fe_3O_4 nanoparticles as enzyme mimics for the sensitive detection of bacteria, *Chem. Commun.*, 2017, **53**(91), 12306.

28 D. Ma, A. Liu, S. Li, C. Lu and C. Chen, TiO_2 photocatalysis for C–C bond formation, *Catal. Sci. Technol.*, 2018, **8**(8), 2030.

29 W. L. Harrigan, S. E. Michaud, K. A. Lehuta and K. R. Kittilstved, Tunable electronic structure and surface defects in chromium-doped colloidal $SrTiO_{3-\delta}$ nanocrystals, *Chem. Mater.*, 2016, **28**(2), 430.

30 Z. Sun, L. Zhang, F. Dang, Y. Liu, Z. Fei, Q. Shao, H. Lin, J. Guo, L. Xiang, N. Yerra and Z. Guo, Experimental and simulation-based understanding of morphology controlled barium titanate nanoparticles under co-adsorption of surfactants, *CrystEngComm*, 2017, **19**(24), 3288.

31 S. Adireddy, C. Lin, B. Cao, W. Zhou and G. Caruntu, Solution-Based Growth of Monodisperse Cube-Like $BaTiO_3$ Colloidal Nanocrystals, *Chem. Mater.*, 2010, **22**(6), 1946.

32 R. H. Mitchell, A. R. Chakhmouradian and P. M. Woodward, Crystal chemistry of perovskite-type compounds in the tausonite-loparite series, $(Sr_{1-2x}Na_xLa_x)TiO_3$, *Phys. Chem. Miner.*, 2000, **27**(8), 583.

33 P. A. Giguère and I. D. Liu, On the infrared spectrum of hydrazine, *J. Chem. Phys.*, 1952, **20**(1), 136.

34 E. J. Bowen and A. W. Birley, The vapour phase reaction between hydrazine and oxygen, *Trans. Faraday Soc.*, 1951, **47**, 580.

35 K. van Benthem, C. Elsässer and R. H. French, Bulk electronic structure of $SrTiO_3$: experiment and theory, *J. Appl. Phys.*, 2001, **90**(12), 6156.

36 K. A. Lehuta and K. R. Kittilstved, Reversible control of the chromium valence in chemically reduced Cr-doped $SrTiO_3$ bulk powders, *Dalton Trans.*, 2016, **45**(24), 10034.

37 F. Zuo, L. Wang, T. Wu, Z. Zhang, D. Borchardt and P. Feng, Self-doped Ti^{3+} enhanced photocatalyst for hydrogen production under visible light, *J. Am. Chem. Soc.*, 2010, **132**(34), 11856.

38 C. Mitra, C. Lin, J. Robertson and A. A. Demkov, Electronic structure of oxygen vacancies in $SrTiO_3$ and $LaAlO_3$, *Phys. Rev. B: Condens. Matter Mater. Phys.*, 2012, **86**(15), 155105.

39 W. D. Rice, P. Ambwani, M. Bombeck, J. D. Thompson, G. Haugstad, C. Leighton and S. A. Crooker, Persistent optically induced magnetism in oxygen-deficient strontium titanate, *Nat. Mater.*, 2014, **13**(5), 481.

40 A. Henglein, Colloidal TiO_2 catalyzed photo- and radiation chemical processes in aqueous solution, *Ber. Bunsenges. Phys. Chem.*, 1982, **86**(3), 241.

41 W. L. Harrigan and K. R. Kittilstved, Reversible modulation of the Cr^{3+} spin dynamics in colloidal $SrTiO_3$ nanocrystals, *J. Phys. Chem. C*, 2018, **122**(46), 26652.

42 E. Carter, A. F. Carley and D. M. Murphy, Evidence for O_2^- radical stabilization at surface oxygen vacancies on polycrystalline TiO_2, *J. Phys. Chem. C*, 2007, **111**(28), 10630.

43 B. Pallavi D, B. Deu S and G. Gavisiddappa S, Visible light active superoxide modified nanocrystalline anatase titania, *J. Nanoeng. Nanomanuf.*, 2015, **5**, 216.

44 Z. Wei, D. Liu, W. Wei, X. Chen, Q. Han, W. Yao, X. Ma and Y. Zhu, Ultrathin TiO_2(B) Nanosheets as the Inductive Agent for Transferring H_2O_2 into Superoxide Radicals, *ACS Appl. Mater. Interfaces*, 2017, **9**(18), 15533.

45 A. L. Attwood, D. M. Murphy, J. L. Edwards, T. A. Egerton and R. W. Harrison, An EPR study of thermally and photochemically generated oxygen radicals on hydrated and dehydrated titania surfaces, *Res. Chem. Intermed.*, 2003, **29**(5), 449.

46 J. Green, E. Carter and D. M. Murphy, Interaction of molecular oxygen with oxygen vacancies on reduced TiO_2: site specific blocking by probe molecules, *Chem. Phys. Lett.*, 2009, **477**(4–6), 340.

47 K. Komaguchi, T. Maruoka, H. Nakano, I. Imae, Y. Ooyama and Y. Harima, Electron-transfer reaction of oxygen species on TiO_2 nanoparticles induced by sub-band-gap illumination, *J. Phys. Chem. C*, 2010, **114**(2), 1240.

48 K. Komaguchi, T. Maruoka, H. Nakano, I. Imae, Y. Ooyama and Y. Harima, ESR study on the reversible electron transfer from O_2^{2-} to Ti^{4+} on TiO_2 nanoparticles induced by visible-light illumination, *J. Phys. Chem. C*, 2009, **113**(4), 1160.

49 H. Möckel, M. Giersig and F. Willig, Formation of uniform size anatase nanocrystals from bis(ammonium lactato) titanium dihydroxide by thermohydrolysis, *J. Mater. Chem.*, 1999, **9**, 3051.

50 G. A. Seisenbaeva, G. Daniel, J. M. Nedelec and V. G. Kessler, Solution equilibrium behind the room-temperature synthesis of nanocrystalline titanium dioxide, *Nanoscale*, 2013, **5**(8), 3330.

51 S. M. Bertolino, L. A. Melgaco, R. G. Sa and V. A. Leao, Comparing lactate and glycerol as a single-electron donor for sulfate reduction in fluidized bed reactors, *Biodegradation*, 2014, **25**(5), 719.

52 V. Vandieken, N. Finke and B. Thamdrup, Hydrogen, acetate, and lactate as electron donors for microbial manganese reduction in a manganese-rich coastal marine sediment, *FEMS Microbiol. Ecol.*, 2014, **87**(3), 733.

53 S. Tsubakizaki, H. Gotou, N. Ishihara, M. Takada, K. Mawatari and R. Kai, Alternatives to hydrazine in water treatment at thermal power plants, *Mitsubishi Heavy Ind. Tech. Rev.*, 2009, **46**(2), 43.

54 B. Scrivenand and T. R. Winter, Chemical oxygen scavengers - Use of hydrazine and tannins for boiler water treatment, *Anti-Corros. Methods Mater.*, 1978, **25**(10), 10.